Visualization of Fast Ion Phase-space Flow Driven by Alfvén Instabilities

X.D. Du,[1] M.A. Van Zeeland,[1] W.W. Heidbrink,[2] J. Gonzalez-Martin,[2] K. Särkimäki,[3] A. Snicker,[4] D. Lin,[2] C.S. Collins,[1] M.E. Austin,[5] G.R. McKee,[6] Z. Yan,[6] Y. Todo,[7] and W. Wu[1]

[1] *General Atomics, P.O. Box 85608, San Diego, California 92186-5608, USA*
[2] *University of California, Irvine, California 92697, USA*
[3] *Department of Physics, Chalmers University of Technology, SE-41296 Göteborg, Sweden*
[4] *Department of Applied Physics, Aalto University, P.O. Box 11100, 00076 AALTO, Finland*
[5] *University of Texas-Austin, Austin, Texas 78712, USA*
[6] *University of Wisconsin-Madison, Madison, Wisconsin 53706-1687, USA*
[7] *National Institute for Fusion Science, 509-5292 Toki, Japan*

(Dated: October 28, 2021)

Fast ion phase-space flow, driven by Alfvén eigenmodes (AEs), is measured by an imaging neutral particle analyzer in the DIII-D tokamak. The flow firstly appears near the minimum safety factor at the injection energy of neutral beams, and then moves radially inward and outward by gaining and losing energy, respectively. The flow trajectories in phase space align well with the intersection lines of the constant magnetic moment surfaces and constant $E-(\omega/n)P_\zeta$ surfaces, where E, P_ζ are energy and toroidal canonical momentum of ions; ω and n are angular frequencies and toroidal mode numbers of AEs. It is found that the flow is so destructive that the thermalization of fast ions is no longer observed in regions of strong interaction. The measured phase-space flow is consistent with nonlinear hybrid kinetic-magnetohydrodynamics simulation. Calculations of the relatively narrow phase-space islands reveal that fast ions must transition between different flow trajectories to experience large-scale phase-space transport.

PACS numbers:

Wave-particle interaction is a universal phenomenon of great importance in physical systems, including astrophysics, laser physics, and many others. In magnetically confined fusion devices, wave-particle resonances can drive massive fast-ion transport across phase space. Predicting and minimizing this transport is a key issue to achieve a sustainable burning plasma in fusion reactors. Past studies measure fast ion profiles, averaging over a broad portion of phase space, to study global confinement [1–7]. However, wave-particle interactions occur locally in phase space and resonant fast ions migrate along certain phase-space routes, something which has not been measured before. Understanding the phase-space flow formation and its evolution are important issues that could impact operation of nuclear fusion reactors. It is fundamental to the development of predictive modeling, control techniques to mitigate fast ion loss and advanced operation scenarios, such as utilizing the alpha channelling effect [8]. Transport by Alfvén eigenmodes (AE) is a particular concern. To address this, an imaging neutral particle analyzer (INPA) [9, 10] was developed in the DIII-D tokamak. The first ever visualization of fast ion phase space flow driven by AEs is reported here.

The INPA measures energetic neutrals, which are produced by charge-exchange reactions between confined fast ions and an active neutral beam source, as seen from Fig. 1(a). The system covers nearly all radii, and resolves the neutral energies from ~ 30 keV to ~ 100 keV. The diagnostic sensitivity or 'weights' of $\sim 1\%$ of the available INPA pixels in the radius-energy plane, depicted as the white circles in Fig. 1(b), are estimated using the synthetic diagnostic code (INPASIM) [11, 12]. Each circle corresponds to the contour lines of 30% of the maximum weights. The INPASIM also finds that fast ions with the pitch $v_\parallel/v$ from ~ 0.77 to 0.84 can be collected by INPA, illustrated as the black band ($v_\parallel$ refers to the fast ion velocity parallel to the magnetic field line). Note that the validation of the INPA system [9, 10] and synthetic modeling [11] in a broad range of plasma parameters were systematically reported in [11, 13].

The orbit topology over the INPA-interrogated phase space, computed by the orbit tracing code (ASCOT5) [14], is overlaid. The system interrogates the phase space occupied by well-confined fast ions on stagnation orbits

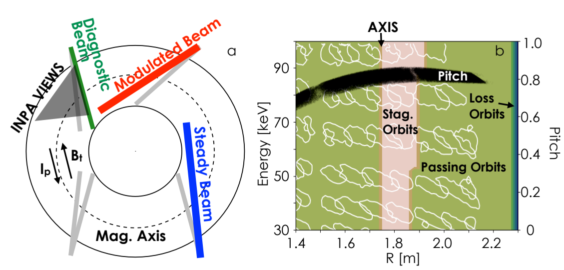

FIG. 1: (a) the neutral beam geometry, along with the INPA view. (b) the weight function of the INPA (circles) on energy-radius plane, along with the measured pitch range. The orbit topology in the INPA-interrogated phase space is overlaid.

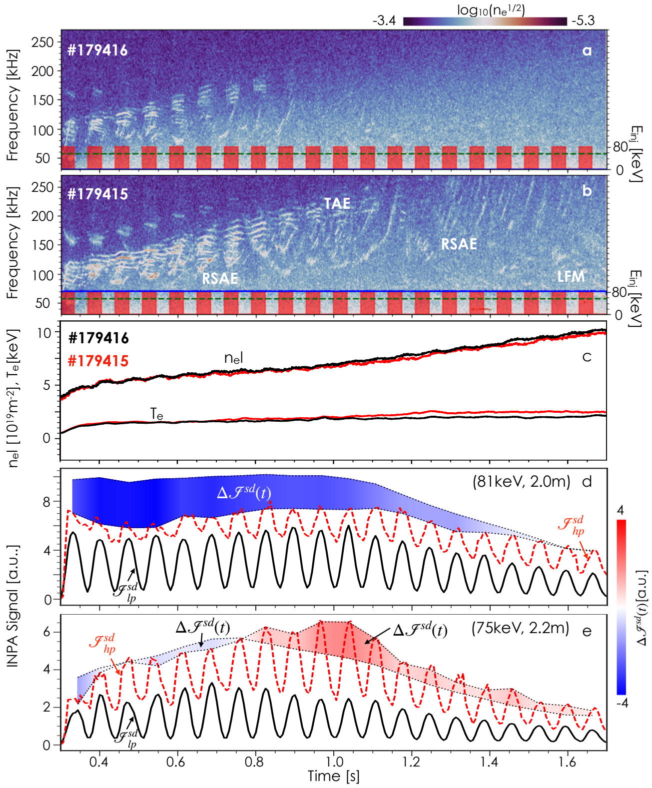

FIG. 2: Frequency spectra of the density fluctuation for the low-power shot (a) and high-power shot (b), along with the waveforms of the neutral beams. (c) The time evolution of line-integrated n_e and T_e. The measured INPA signal in the low-power shot (solid line) and high-power shot (dashed line) and the signal deficit to the expectation of the neoclassical theory (colormap) for the velocity space ($E \sim 81$ keV , $R \sim 2.0$ m) (d) and ($E \sim 70$keV , $R \sim 2.2$ m) (e).

near the magnetic axis and on passing orbits elsewhere. Stagnation orbits are a class of orbits which are confined on a given side of the magnetic axis near the device midplane which travel in a single toroidal direction. The view does not cover the confined-loss boundary.

A controlled experiment is designed to visualize the phase-space flow in the plasma current ramp-up phase, at a toroidal magnetic field of ~ 2.1 T and in an upper single null magnetic configuration. The strategy is to vary AE activities in a pair of shots as much as possible, with a minimum change of the plasma parameters and equilibrium. As seen from Fig. 2(a), the plasma with less or no AE activity in the low-power (lp) shot (#179416) is heated by two neutral beams, i.e., a steady diagnostic neutral beam at 55 keV of 1 MW and a modulated beam at 81 keV of 2.5 MW with a cycle time of 70 ms and a duty cycle of 50%. The INPA detects the charge-exchanged neutral flux from a time-evolving slowing-down (sd) fast ion distribution. That is, the image above 55 keV can be expressed as $\mathcal{I}_{\rm lp} \equiv \mathcal{I}^{\rm sd}_{\rm lp}(t)$.

The AE activity in Fig. 2(b) are largely enhanced after adding a steady (st) beam of $\sim$ 82 keV at a modest beam power of $\sim$ 1.7 MW. The beam is injected at the axisymmetry angle of the modulated beam. Thus, the image in the high-power (hp) shot can be expressed as, $\mathcal{I}_{\rm hp} \equiv \mathcal{I}^{\rm sd}_{\rm hp}(t) + \mathcal{I}^{\rm st}_{\rm hp}$, where $\mathcal{I}^{\rm st}_{\rm hp}$ is the image produced by the steady beam.

As seen from Fig. 2(c), the electron density n_e agrees well in the pair of shots, due to a delicate tuning of the n_e feedback control system. The electron temperature T_e also agrees well before $\sim$ 1.0 s, and starts to deviate later. In this circumstance, neoclassical theory expects $\mathcal{I}^{\rm sd}_{\rm lp}(t) = \mathcal{I}^{\rm sd}_{\rm hp}(t)$. This is experimentally demonstrated by a quantitative agreement of $\mathcal{I}^{\rm sd}_{\rm lp}(t)$ and $\mathcal{I}^{\rm sd}_{\rm hp}(t)$, when AEs are stable, and further supported by the agreement with synthetic INPA images, using the fast ion distribution predicted by NUBEAM module of TRANSP [15]. For details, see the Supplemental Material [16].

As expected, when AEs are unstable, $\mathcal{I}^{\rm sd}_{\rm lp}(t)$ and $\mathcal{I}^{\rm sd}_{\rm hp}(t)$ deviate. Figures 3 and 4 compare images at two different modulation periods in these two discharges. In Fig. 3 at $\sim$ 1.0 s , the AE activity is absent in low-power shot and relatively weak in high-power shot (see Fig. 3(a4) and (b4)); while in Fig. 4 at $\sim$ 0.38 s, the AE activity appears even in low-power shot and is quite strong in high-power shot (see Fig. 4(a4) and (b4)). In both cases, three snapshots at three different times in the beam modulation cycle are shown to illustrate the birth and subsequent slowing-down of ions from the modulated source. Even when the AE activity is relatively weak, noticeable differences between images in the two shots appear (Fig. 3). Although the n_e profiles match, less full-energy fast ions appear in the plasma core in the high-power shot. Moreover, in spite of a slightly higher edge T_e by $\sim$ 10 % in the high-power shot, more INPA signal appears at the reduced energy of $\sim$ 75 keV at $R > 2.1$ m, as indicated by the arrows. These features are in contrast to expectations from neoclassical theory, which would predict: (i) for the same density profile, the ionization profile of fast ions is expected to be the same; (ii) for a higher edge T_e, the slowing-down time is longer and thus less INPA signal at the lower energy range is expected for the high power shot. For convenience, the red (blue) colored region in Fig. 3(c1)-(c3) are called an inflow (outflow) region, where the amount of the confined fast ions are above (below) that in the low-power shot.

The deviation of $\mathcal{I}^{\rm sd}_{\rm lp}(t)$ and $\mathcal{I}^{\rm sd}_{\rm hp}(t)$ is even more significant, when the AE activity is strong (Fig. 4). The differences are: (i) The INPA signal of the modulated beam at the injection energy of 82 keV, indicated by the dotted lines, is mostly missing in the high-power shot, as seen from Figs. 4(b1)-(b3). It suggests a full depletion of ionized neutrals in a time scale much shorter than the camera integration time of 0.5 ms. That is, when AEs are unstable even in the low-power shot (see Fig. 4(a4)), the phase space in high-power shot exhibits strong self-organized criticality dynamics. (ii) The slowing-down of

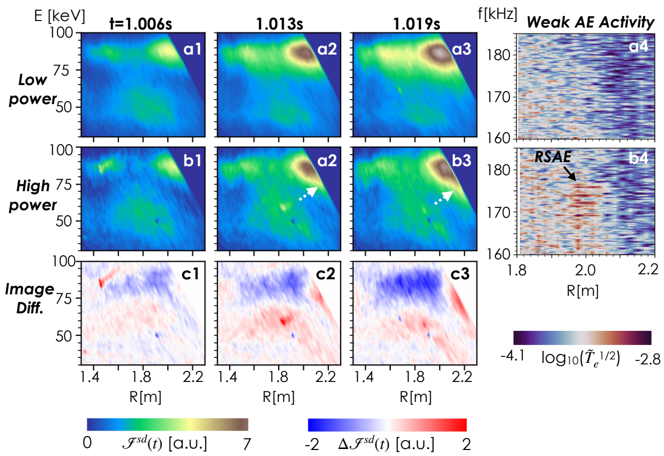

FIG. 3: INPA images of the modulated beam source during the weak AE activity (from 1.006s to 1.019s). (a1)-(a3) Low power shot 179416. (b1)-(b3) High power shot 179415. (c1)-(c3) Difference image. T_e fluctuation in low-power shot (a4) and in high-power shot (b4) at ~ 1.013 s.

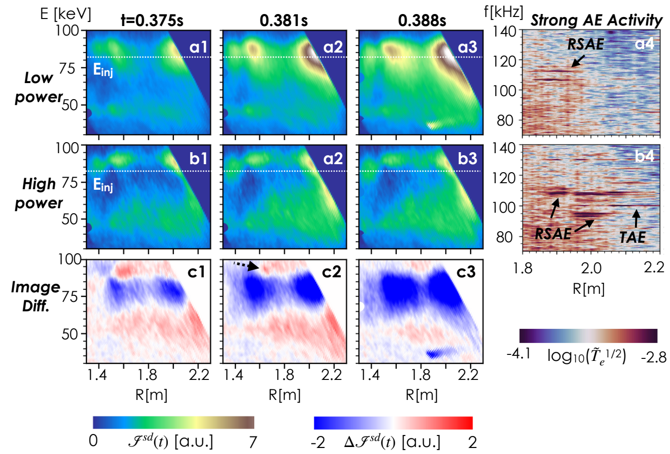

FIG. 4: INPA images of the modulated beam source during strong AE activity (from 0.375s to 0.388s). (a1)-(a3) Low power shot 179416. (b1)-(b3) High power shot 179415. (c1)-(c3) Image differnece. T_e fluctuation in low-power shot (a4) and high-power shot (b4) at ~ 0.381 s.

fast ions is not observed across the image series in the high-power shot, which is consistent with the fact that the increase of T_e is barely noticeable in the plasma core after adding neutral beam power of 1.7 MW (see Fig. 2(c)). (iii) As seen from the highlighted image differences $\Delta\mathcal{I}^{\rm sd}(t) \equiv \mathcal{I}^{\rm sd}_{\rm hp}(t) - \mathcal{I}^{\rm sd}_{\rm lp}(t)$ in Fig. 4(c1)-(c3), an inflow region (red) in the plasma core emerges, as indicated by the arrow. It shows radially inward transport of fast ions with energies exceeding the injection energy of 82 keV . It should be mentioned that the image pattern of the $\Delta\mathcal{I}^{\rm sd}(t)$ smoothly evolves, as AEs activities are gradually diminishing from 0.3 s to 1.7 s.

These changes in $\Delta\mathcal{I}^{\rm sd}(t)$ depend on the strength of the AE activity. Figures 2(d) and 2(e) show the time evolution of the flows for two INPA pixels. For a pixel near the radius of the strongest AE activity ($R = 2.0$ m) near the injection energy of ~ 81 keV, strong outflow is observed that steadily decreases as the AE activity weakens in time (see Fig. 2(d)). For a pixel at lower energy and larger radius, inflow occurs for intermediate levels of AE activity, then ceases when the AEs become stable (see Fig. 2(e)). No inflow is observed during the early phase of very strong AE activity at the end of modulation periods. During this phase, the strong edge toroidicity-induced AE (TAE) activity (see Fig. 4(b4)) prevents redistribution of fast ions in the outer region of $R > 2.1$ m at reduced energy of $E < 75$ keV.

To understand the connection of the observed inflow (red) and outflow (blue) areas across the phase space, fast ion migration trajectories are reconstructed, referred to as the streamlines below. It is known that the magnetic moment μ is conserved during resonant interactions with AEs as long as the AE frequency is much lower than the ion cyclotron frequency. Moreover, $E' \equiv E - \omega P_\zeta/n$ is also conserved [7], where P_ζ is the toroidal canonical momentum; ω and n are the angular frequency and toroidal mode number of the AE, respectively. To simultaneously satisfy the constraints, the streamline must follow the intersection of the curved, constant μ and E' planes in phase space. The curved μ and E' planes in the coordinate (E, R, $v_\parallel/v$) are calculated by ASCOT5 and the intersection of two planes, i.e., $E'\&\mu$ streamlines, is identified. Owing to the finite pitch ($v_\parallel/v$) resolution discussed in Fig. 1(b), a majority part of the $E'\&\mu$ streamlines may intersect the phase space volume interrogated by the INPA. By scanning μ and E', and all observed ω/n, we reconstruct the streamlines in the INPA views, given as the dotted lines in Fig. 5(a). The streamline, associated with dominant reversed-shear AE (RSAE), having $n = 2$, $l = 0$, $f = 86$ kHz in plasma frame, is labeled as b1; the streamlines of RSAE with $n = 2$, $l = 1$ and $f = 89$ kHz for two E' constants are given as b2 and b3. (l: the number of nodes in the radial eigenmode envelope). Note that these streamlines are most relevant to the observed image pattern, since they pass through the radial positions of the minimum safety factor q_{min} at $R \sim 2.0$ m near the beam injection energy, and connect the outflow region and two inflow regions together. Besides, the majority part of streamlines, related to edge TAEs with lower ω/n, does not intersect the INPA-interrogated phase space and only a small portion appears well below the injection energy.

The phase-space flow is further investigated, using a nonlinear, kinetic-magnetohydrodynamics (MHD) hybrid code (MEGA) [17–19]. The simulation uses the measured plasma profiles, the equilibrium reconstructed by EFIT [20] and fast ion distributions ($\mathcal{F}_{\rm fi}$) from NUBEAM module of TRANSP [15] at ~ 0.44 s as the initial conditions. The $\mathcal{F}_{\rm fi}$ evolves in three separated periods in the

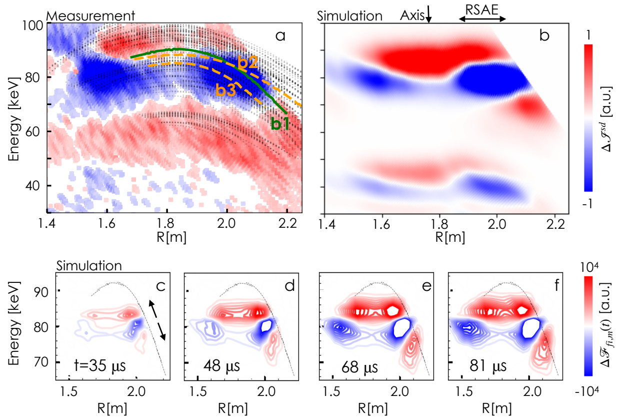

FIG. 5: (a) The measured flow images in (a), along with the streamlines; (b) the simulated flow image using MEGA-estimated fast ion distributions at INPA measured pitch of ~ 0.78; time evolution of the fast ion distributions in (c)-(f) by MEGA simulation.

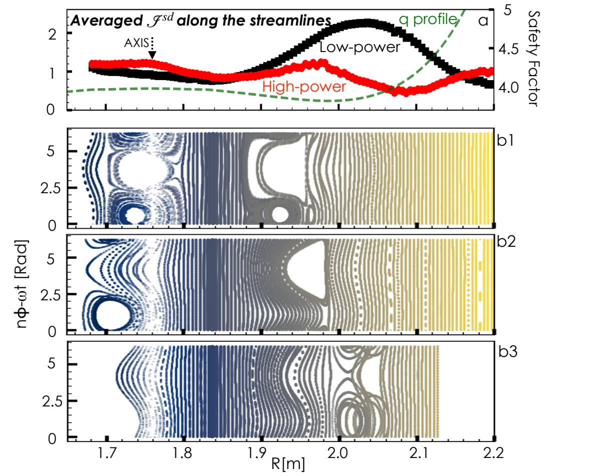

FIG. 6: (a) The averaged INPA signal along the streamlines b1-b3 in Fig. 5 in the LP shot (black) and in the HP shot (red), along with the q profile. The estimated phase-space islands along these streamlines b1-b3 in (b1)-(b3), respectively.

absence of MHD instabilities. This is to simulate the fast ion thermalization process. Following each period, the kinetic-MHD hybrid phases are conducted subsequently for 0.1 ms and the RSAEs of n=2 are routinely identified. Meanwhile, the $\mathcal{F}_{\rm fi,m}$, i.e., the fast ion distribution related to the modulated beam, is largely modified at INPA interrogated pitch of 0.78. As one example, figures 5(c)-(f) present the change of $\mathcal{F}_{\rm fi,m}$ at 35, 48, 68 and 81 μs after RSAE excitation in the third hybrid phase. It is found that the outflow (blue) and the inflow (red) region expands along the streamline, revealing formation of RSAE-driven, fast ion phase space flow. Here, the streamline b1, indicated by the black curve, is overlaid as the reference. The synthetic INPA image in Fig 5(b) is obtained by a convolution integral of the $\mathcal{F}_{\rm fi,m}$ at 81 μs and the computed weight function. The result reproduces the observed inflow (red) and outflow (blue) regions in phase space, showing a reasonable agreement with the averaged $\Delta\mathcal{I}^{\rm sd}$ images in Fig. 5(a). It is worth pointing out that the further expansion of the outflow (blue) region towards the boundary of INPA view (see Fig 4(c3)), caused by the edge TAE modes, has not been reproduced by MEGA. The discrepancy below 60 keV is also speculated to be due to the lack of the TAE modes, which will be addressed in future work.

AEs flatten the fast ion-density along $E'\&\mu$ streamlines. The $\mathcal{I}^{\rm sd}_{\rm lp}$, averaged over the labeled streamlines in Fig. 5(a), shows a hollow profile with a peak near the $q_{\rm min}$ location at $R = 2.0$ m in the low-power shot, as seen from the black line in Fig. 6(a). This is because the neutral beam nearly tangential to the magnetic field line populates the magnetic axis region with a pitch of ~ 0.68, outside of the INPA-interrogated pitch [10]. In contrast, the $\mathcal{I}^{\rm sd}_{\rm hp}$ in the high-power shot is significantly flattened along the streamline (red line in Fig. 6(a)).

To understand the transport mechanism, the phase-space islands along the labeled streamlines b1-b3 in Fig. 5(b) are studied using ASCOT5 code [14] and the results are given in Figs. 6(b1) -(b3). These island chains are generated by the wave-particle resonant interactions and visualized by the Poincaré plots of fast ions orbits in presence of RSAE modes. Fast ions with constant $\mu = 18$ keV/T, interrogated by the INPA, are launched along the streamlines from the midplane. The radial structures of RSAE are obtained by a kinetic-MHD stability analysis code (NOVA-K) [21] and selected accordingly, based on the T_e fluctuation measured by electron cyclotron emission (ECE) [22]. The amplitude of each AE is carefully calibrated using magnetic field line tracing technique, which is able to determine the magnetic perturbation from the measured $\tilde{T}_e$ profiles by mapping constant T_e along magnetic field lines. Note that the transient maximum amplitude of AEs are used, instead of the averaged value from Fast Fourier transform.

As seen from Figs. 6(b1)-(b3), good Kolmogorov-Arnold-Moser surfaces widely exist along each streamline. In other words, fast ions cannot flow freely along a single streamline to travel across the system. On the other hand, the observed flattening region is much broader than the widths of the phase-space islands. This contradiction suggests that fast ions cross between streamlines to achieve the large-scale phase space flow. One mechanism of streamline crossing is the natural intersection of streamlines with different values of ω/n. For example, the intersection of streamlines b1 and b2 would increase the phase-space flow traveling distance by 8 cm, as seen in Fig. 6(b1) and (b2); A second mechanism is scattering by collisions or turbulence from one streamline to a neighboring streamline of different radial extent. For example, the streamline b2 and b3 from the same RSAE are close to each other in Fig. 5(a). However, their phase space islands drift by ~ 8 cm, as seen from Fig. 6(b2) and (b3). It is hypothesized that the intermittency of fast ion avalanche transport [23] may be due to the sudden increase of the streamline crossing, either by the transient excitation of new instabilities or the randomized turbulence.

In summary, the first ever visualization of fast ion phase space flow driven by AEs is reported here. It is found that the phase space flow is a 'two-way traffic' i.e., inward transport towards higher energy and outward transport to reduced energy, determined by relative velocity of fast ions and their initial positions to the waves during resonant interactions. The result is consistent with non-linear kinetic-MHD hybrid simulations. For the first time, flattening of the fast ion distribution function along $E'\&\mu$ streamlines has been directly measured. When AEs are unstable even in the low-power shot, the phase space along the streamline shows strong self-organized criticality dynamics in high-power shot, i.e., an open system with a fast relaxation mediation by the threshold [24]. The transport along the streamline is compared to the widths of phase-space islands, generated by the resonant interactions with AEs. The result shows that streamline crossing, either due to the natural intersection of streamlines or small pitch-angle scattering by turbulence or collisions, plays a key role for the large-scale phase-space transport.

The author (X.D. Du) would like to thank M. Podestà, G.J. Kramer and R.Nazikian for fruitful discussions. This work was supported by the US DOE under DE-AC05-00OR22725, DE-FC02-04ER54698, DE-AC02-09CH11466, DE-SC0015878. The ASCOT5 project has received funding from the European Research Council under the European Union's Horizon 2020 research and innovation program under grant agreement No 647121.

[1] W.W. Heidbrink and G.J., Sadler, Nucl. fusion 34, 535 (1994).
[2] A. Fasoli, C. Goremnzano, H.L. Berk et al., Nucl. Fusion 47, S264 (2007).
[3] B.N. Breizman and S.E. Sharapov, Plasma Phys. Controlled Fusion 53, 054001 (2011).
[4] TOI, K., OGAWA, K., ISOBE, M., et al., K. Toi, K. Ogawa, M. Isobe et al., Plasma Phys. Controlled Fusion 53, 024008 (2011).
[5] N.N. Gorelenkov, S.D. Pinches, K. Toi, Nucl. Fusion 54, 125001 (2014).
[6] K. Mcclements and E.D. Fredrickson, Plasma Phys. Controlled Fusion 59, 053001 (2017).
[7] Y. Todo, Reviews of Modern Plasma Physics (2019) 3:1 (2019).
[8] N. J. Fisch, Phys. Rev. Lett. 41, p. 873 (1978)
[9] X.D. Du, M.A. Van Zeeland, W.W. Heidbrink and D. Su, Nucl. Fusion 58, 082006 (2018).
[10] M.A. Van Zeeland, X.D. Du, W.W. Heidbrink, L. Stagner, and D. Su, JINST 14, C09027 (2019).
[11] X.D. Du, M.A. Van Zeeland, W.W. Heidbrink and L. Stagner and D. Su, Nucl. Fusion 60, 112001 (2020).
[12] W.W. Heidbrink, D. Liu , Y. Luo, E. Ruskov and B. Geiger, Commun. Comput. Phys. 10 716 (2011).
[13] D.J. Lin, X.D. Du, W.W. Heidbrink and M.A. Van Zeeland, Nucl. Fusion 60, 112008 (2020).
[14] E. Hirvijoki, O. Asunta, T. Koskela, T. Kurki-Suonio, J. Miettunen, S. Sipila, A. Snicker, S. Akaslompolo Computer Physics Communications 185,1310–1321 (2014).
[15] Pankin A., Mccune D., Andre R., Bateman G. and Kritz A. Comput. Phys. Commun. 159 157 (2004).
[16] See supplemental Material [url] for INPA images without AE activities, which includes references [11–13, 15, 25, 26].
[17] Y. Todo and T. Sato., Phys. Plasmas 5, 1321–7 (1998).
[18] Y. Todo, H. Berk and B. Breizman Nucl. Fusion 50, 084016 (2010).
[19] Y. Todo, R. Seki, D.A. Spong, H. Wang, Y. Suzuki, S. Yamamoto, N. Nakajima and M. Osakabe, Phys.Plasmas 24, 081203 (2017)
[20] L. Lao, H. St John, R. Stambaugh, A. Kellman and W. Pfeiffer, Nucl. Fusion 25, 1611(1985).
[21] C. Z. Cheng, Phys. Rep. 1, 211 (1992).
[22] M.A. Van Zeeland, G.J. Kramer, M.E Austin, R.L Boivin, W.W.Heidbrink, M.A. Makowski, G.R. McKee, R. Nazikian, W.M. Solomon, G. Wang, Phys. Rev. Lett. 97, 135001 (2006).
[23] C.S. Collins, W.W. Heidbrink, M.E. Austin, G.J. Kramer, D.C. Pace, C.C. Petty, L. Stagner, M.A. Van Zeeland, R.B. White, Y.B. Zhu, Phys. Rev. Lett. 116, 095001 (2016).
[24] R. Sanchez and D.E. Newman, Plasma Phys. Control. Fusion 57, 123002 (2015).
[25] W.W. Heidbrink, M.A. Van Zeeland, M.E. Austin, A. Bierwage, Liu Chen, G.J. Choi, P. Lauber, Z. Lin, G.R. McKee and D.A. Spong, Nucl. Fusion 61, 016029 (2021)
[26] G.J. Choi, P. Liu, X.S. Wei, J.H. Nicolau, G. Dong, W.L. Zhang, Z. Lin, W.W. Heidbrink and T.S. Hahm, Nucl. Fusion 61, 066007 (2021).